A fast luminosity monitor based on diamond detectors for the SuperKEKB collider

C.G. Pang, P. Bambade, S. Di Carlo, Y. Funakoshi, D. Jehanno, V. Kubytskyi, M. Masuzawa, Y. Peinaud, C. Rimbault, S. Uehara

A Fast Luminosity Monitor based on diamond detectors for the SuperKEKB Collider

C. G. Pang[a,*], P. Bambade[a], S. Di Carlo[a], Y. Funakoshi[b], D. Jehanno[a], V. Kubytskyi[a], M. Masuzawa[b], Y. Peinaud[a], C. Rimbault[a], S. Uehara[b]

[a] *LAL, Univ. Paris-Sud, CNRS/IN2P3, University Paris-Saclay, Orsay, France*
[b] *KEK, 1-1 Oho, Tsukuba, Ibaraki 305-0801, Japan*

Abstract

A fast luminosity monitor measuring the rate of the radiative Bhabha process at zero degree photon scattering angle based on diamond detectors was developed and successfully operated during the Phase-2 commissioning of SuperKEKB. The main purpose of this system, called LumiBelle2 is to provide: train integrated luminosity signals at 1 kHz with a relative precision better than 1% for luminosities higher than $10^{34}\ cm^{-2}s^{-1}$, input to a dithering feedback system designed to maintain an optimum horizontal overlap between the two colliding beams at the Interaction Point (IP), and bunch integrated luminosity signals at 1 Hz which are useful for machine tuning and beam parameters studies of the successive bunches along the train. In this paper, design of the LumiBelle2 and Phase-2 results will be reported, including the evaluation of the single beam background, relative luminosity measurements, vertical beam size determinations at the IP using vertical offset scans.

Keywords: luminosity, radiative Bhabha, sCVD diamond detector, beam instrumentation, dithering feedback, SuperKEKB

*Corresponding author
Email address: pang@lal.in2p3.fr (C. G. Pang)

1. Introduction

SuperKEKB is an asymmetric e^+ e^- collider [1, 2] at KEK, Japan, designed to provide very high luminosity for the Belle II experiment [3]. With the concept of the "nano-beam scheme" and doubled beam currents, implemented by colliding highly focused ultra-low emittance bunches every 4 ns, it is expected that it will achieve a luminosity (8×10^{35} $cm^{-2}s^{-1}$) 40 times higher than that of KEKB, thus becoming the highest luminosity particle collider that have ever existed.

A particle collider with such small beam sizes requires strict control of the beam orbits at the Interaction Point (IP) to ensure that an optimum geometrical overlap is maintained between the two colliding beams. In the presence of horizontal ground motion, the offset between the two beams at the IP can become large enough to significantly degrade the luminosity [4]. The sensitivity to the horizontal offsets is enhanced through the hourglass effect, due to the very small vertical β_y^* (≈ 300 μm) at the IP and large horizontal crossing angle (83 mrad). To maintain very high luminosity in the presence of ground motion, a dithering orbit feedback system similar to that operated in the past at PEP-II [5, 6] is employed to stabilize the horizontal beam orbit at IP, which consists of a fast luminosity monitoring system, lock-in amplifier, dithering magnets and closed orbit correction magnets.

The needed precision of the fast luminosity signals was studied with the nominal beam parameters, showing that a relative precision about 1% for the 1 kHz train integrated luminosity signals ensures that the average luminosity loss caused by horizontal beam-beam offsets would not exceed 0.5% [7].

Single crystal Chemical Vapor Deposition (sCVD) diamond detector, was chosen for the design of LumiBelle2 [8, 9] in view of its high charge carrier mobility and wide band gap, resulting in fast signal formation and good radiation tolerance [10]. Two combinations: diamond detector with dimension of $4\times4\times0.14$ mm^3 coupled with a broadband current amplifier and diamond detector ($4\times4\times0.5$ mm^3) coupled with a fast charge amplifier bought from CIVIDEC

[11], are used. The detectors are installed about 10 and 30 m downstream of the IP in Low Energy Ring (LER) and High Energy Ring (HER), respectively.

The luminosity is monitored by recording the rate of the radiative Bhabha scattering events at vanishing angle, which is proportional to the luminosity and involves a very large cross section ($\sim$ 200 mbarn) [12]. Due to the geometry of the beam lines and the space available, only Bhabha positrons and photons are detected, using diamond detectors installed in the LER and HER, respectively.

As a cross-check and complementary device, another fast luminosity monitoring system, called the Zero Degree Luminosity Monitor (ZDLM), based on Cherenkov and scintillator detectors, was installed in the immediate vicinity of the diamond detectors [9, 13]. The Belle II experiment also measures the absolute luminosity, however at a lower speed, using its electromagnetic end-cap calorimeters to record the coincidence rates in the opposite sectors for Bhabha events with finite scattering angles [14].

In this paper, we describe the LumiBelle2 design of the fast luminosity monitor based on diamond detector, and report on its results in the Phase 2 commissioning period of SuperKEKB, during which beams were collided for the first time. The main results include an evaluation of the single beam background, relative luminosity signals (train integrated luminosity and bunch integrated luminosity), and vertical beam size determinations at the IP using offset scans. A detailed simulation including Bhabha generation, particle tracking and energy deposition in the detector based on Guinea-Pig++ [15], SAD [16], and GEANT4 [17] was used for comparisons with the experimental results and evaluation. Results of the preliminary tests of the dithering feedback system, using both LumiBelle2 and ZDLM 1 kHz luminosity signals as input, are described elsewhere [13, 18].

2. Design and layout

Three detectors were installed in each ring (10 and 29 m downstream of the IP, in the LER and HER, respectively). These positions were carefully studied

to enable fast luminosity monitoring with enough event rates from the radiative Bhabha process to achieve the aimed relative precision in previous study [19]. To enable detecting enough Bhabha scattering events in the LER, a custom made window inclined at 45°, with a depression of 15 mm [9] (see lhs of Figure 1), and including a Tungsten radiator with an effective thickness of 4 Radiation Lengths (1 RL=3.5 mm) was installed at the chosen position: 10 m downstream of the IP. This was very effective to increase the multiplicity of the secondary particles in the showers generated by particles exiting the beam pipe at that location, and thereby the diamond detectors' detection efficiency for Bhabha scattered positrons.

2.1. Mechanical set-up

The mechanical set-up for the luminosity monitoring system consists of pillars in each ring, as shown in Figure 1 (lhs for LER and rhs for HER). Three diamond detectors were installed in each ring. Due to different signal acceptances in each ring, different detectors were installed. In the LER, Bhabha positrons have energies less than the nominal beam energy (4 GeV) and are therefore over-focused and over-bent by the quadrupole and bending magnets after the IP, respectively. A fraction of them of about 10% are lost on 45° window installed 10 m after the IP. Two thin diamond detectors (thickness: 140 μm), coupled with broadband current amplifiers, and one thicker detector (thickness: 500 μm), coupled with fast charge amplifier, were installed. In the HER, two 500 μm and one 140 μm thick diamonds were used to detect photons from Bhabha scattering, coupled with charge and current amplifiers, respectively. All diamond detectors used were 4 mm^2 pads of single crystal CVD diamond bought from CIVIDEC [11]. The charge and current amplifiers were also bought from CIVIDEC [11]. The first detector in the LER is associated with a remotely controlled motor to scan in the horizontal plane over a range of 25 mm.

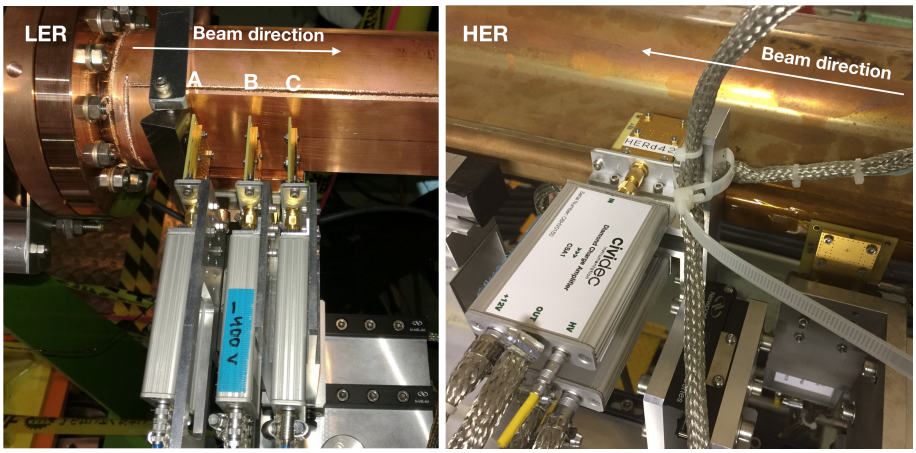

Figure 1: Experimental layout in both ring (lhs: LER, rhs: HER)

2.2. Diamond detectors and amplifiers

The broadband current amplifiers were employed to preserve the timing characteristics of the signals from diamond detector with thickness of 140 μm. The signal amplitude is proportional to the charge generated in the diamond detector by ionization, which is proportional to the number of particles detected at minimum ionization (MIPs). The rise time of the signal pulses is peaked at 0.88 ns, allowing sampling at the peak position after careful phase adjustment. Most of the signal pulses have a full width less than 4 ns, which ensures reasonable measurements of the baseline after each pulse even when signal pulses are present at every bunch crossing, separated nominally by 4 ns [8].

The characteristics of the linear relationship between amplitude and charge, almost fixed rise time and narrow full width of the signals for the 140 μm diamond detector coupled with a broadband current amplifier make this set-up a very good candidate for the front-end of the fast luminosity monitoring system of SuperKEKB [20].

2.3. Data acquisition system

Data acquisition system for our luminosity monitor is located in the Belle-II electronics Hut, where the signals from the detectors are brought via long (about

100 m) half inch thick HELIAX coaxial cables, which significantly reduce both the signals attenuation and dispersion.

The functional diagram is shown in Figure 2. Four among six incoming signals are selected and fed to a 1 GSPS 10-bit AC-coupled ADC board (FMC126, 4DSP), requiring a clock at 1 GHz ($2\times f_{RF}$). The four ADC digital outputs are fed to a VIRTEX-7 FPGA board (VC707, Xilinx): which calculates the train integrated luminosity signals (TIL) over all the bunches in the whole ring, bunch integrated luminosity signals (BIL), counts (event rate) and Rawsum (direct summing all samples) variables in real time, at the rate of up to 1 kHz, for the four CVD inputs, simultaneously. The DAQ also contains a 16-bit DAC, providing 8 analog outputs with 1 kHz bandwidth, that can be configured independently for any of the four input channels.

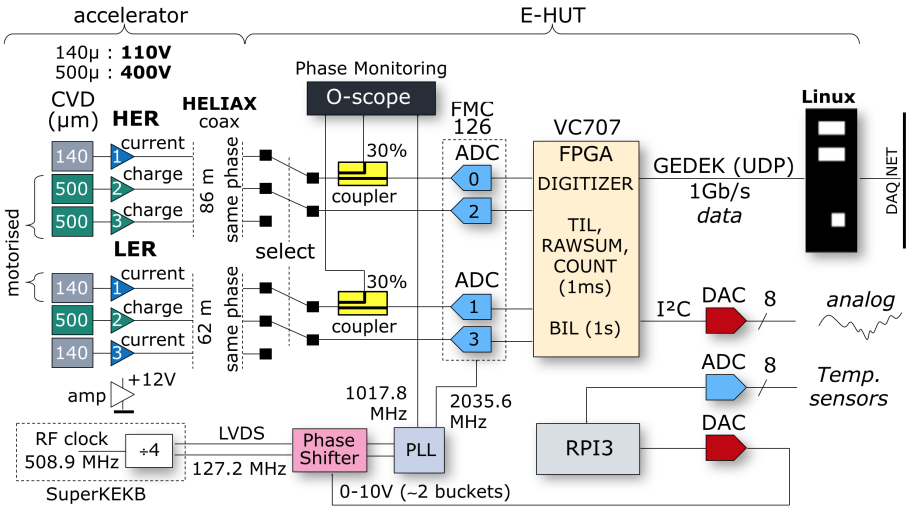

Figure 2: DAQ functional diagram

The DAQ was initially designed to handle a maximum rate of one bunch each 2 ns (all buckets filled). It makes use of two principles: (1) the luminosity is proportional to the amplitudes and rates of signal peaks, and (2) the pulses and RF clock are synchronous, to enable sampling all peaks simultaneously. As the ADC is AC-coupled, the mean value of the pulse train is always centered at 0 V,

requiring therefore to sample also the baseline between subsequent pulses. For bunches separated by 2 ns, this implies sampling at twice of the RF frequency, as illustrated in Figure 3.

Although the amplifiers are not quite fast enough to sample both the signal peaks and baseline for pulses separated by 2 ns, they are adequate for the 4 ns separation planned nominally at SuperKEKB (quasi-2 bucket fill mode). The following rule applies: one sample (1) is positioned on the peak (the phase shifter in Figure 2 is used to find the optimum phase) and the baseline is obtained from the third sample (+3 ns). The luminosity process integrates over 1 ms the sum of all the successive differences Diff(n) of these samples, taking into account a user-defined threshold, to provide the TIL value. The same process provides 5120 sums each 1 second corresponding to the BIL value for each bucket. The Rawsum value calculates the sum of all samples above a defined threshold and is intended for channels using charge amplifiers, which have a shaping time of about 15 ns FWHM. All the real-time data are uploaded to a Linux machine through the GEDEK protocol (ALISE) over an UDP link at 1 GB/s, then converted into nTuple files and saved together with a number of relevant machine parameters available through the EPICS protocol and important for the offline analysis. A subset of the luminosity data were also uploaded to EPICS at a rate of about 1 Hz, for continuous display in the accelerator and Belle II control rooms. Moreover, for the purpose of the IP dithering orbit feedback, analog information from the DAC based on the 1 kHz TIL data was directly fed to the lock-in amplifier used by that system.

Different from other monitoring systems, there is no trigger needed for our DAQ to operate: after careful synchronization to the RF clock of the accelerator, continuous monitoring can be achieved. Due to the large difference in geometry in the HER, comparing with the LER, only Bhabha photons are detectable in the HER, with signal rates about three orders of magnitude lower [9]. While such lower rates will be useful when the highest luminosities which be reached, enabling the desired 1%-level precision at 1 kHz needed for the dithering feedback system, during the Phase-2 commissioning, the rates from

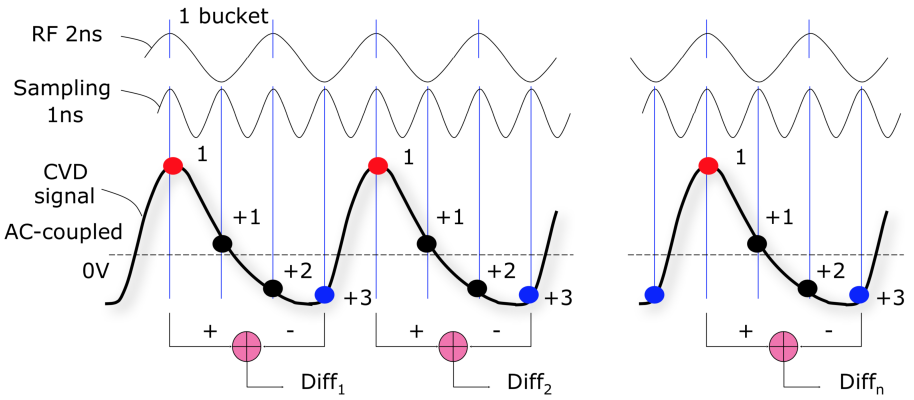

Figure 3: Illustration of DAQ signal processing for 4 ns bunch spacing

the HER were very small and did not provide high statistics for detailed quantitative studies. For this reason, most of the results reported in this paper are from the LER, even if similar studies were also done for the HER demonstrated its full operability.

3. Luminosity monitoring

Phase-2 commissioning of SuperKEKB consisted of single and colliding beam studies. During the single beam studies, our luminosity monitor worked as a beam loss monitor. It detected single beam loss in its immediate vicinity caused by Bremsstrahlung, Touschek and Coulomb scattering processes occurring at various locations upstream, in particular around the IP [21, 22]. With colliding beams, very forward Bhabha scattering events became the luminosity signal and single beam losses the backgrounds.

3.1. Single beam background

Single beam losses caused by Bremsstrahlung, Touschek and Coulomb scattering processes are distributed all over the ring. To study the single beam losses which were the backgrounds for the luminosity monitor, detailed simulations were pursued including generation of the particle scattering [23], tracking to the position of the diamond detector with SAD, as well as a standalone and

realistic 3-D model of the custom made window shape beam pipe and Tungsten radiator, based on GEANT4 to simulate the particles detected by the diamond detectors.

3.1.1. Backgrounds simulation

In the LER, positrons scattered with energies less than the nominal 4 GeV beam energy will be over-deflected by the three bending magnets after the IP, which can cause them to reach the inclined vacuum window at 10 m and thus detected in the detectors, Bremsstrahlung and Touschek processes dominate the background rates in our diamond detectors because they involve scattering of particles with energies less than the nominal one, while for Coulomb scattering, which is an elastic scattering process between beam particles and nuclei of residual gas atoms, scattered positrons only change their direction while keeping their momentum. In the background signal, the contribution from the Coulomb scattering process is less than 1% according to the simulation. In Figures 4 and Figure 5, the energy spectrum and the rate of scattering as function of energy and scattering position, for positrons lost on the window, as shown, for the Bremsstrahlung and Touschek processes, respectively. Scattering position 0 corresponds to the IP and the direction from negative to positive represents the beam direction in the LER. The Energies of the scattered positrons are mainly between 3 and 3.5 GeV, and their scattered positions are mainly distributed around the IP. Especially for the Bremsstrahlung process, the loss rate of which is proportional to the product of the beam current, pressure and square of the effective atomic number of the residual gas in the vacuum beam pipe [24], because of the much narrower beam pipe and absence of vacuum pumps very close to the IP, the vacuum pressure near the IP is about two orders of magnitude higher than the local averaged pressure about 15 m upstream, and the effective atomic number is 4.5 according to a detailed simulation study [25].

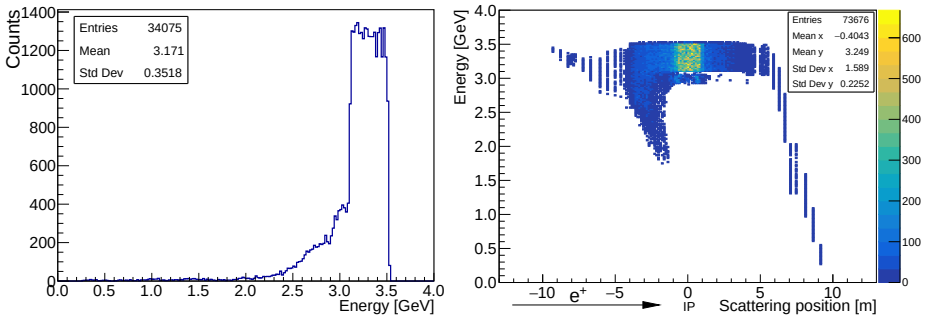

Figure 4: Simulated energy spectrum of Bremsstrahlung positrons lost in the window on l.h.s and their relative rates (in arbitrary units) as function of energy and scattering position on r.h.s.

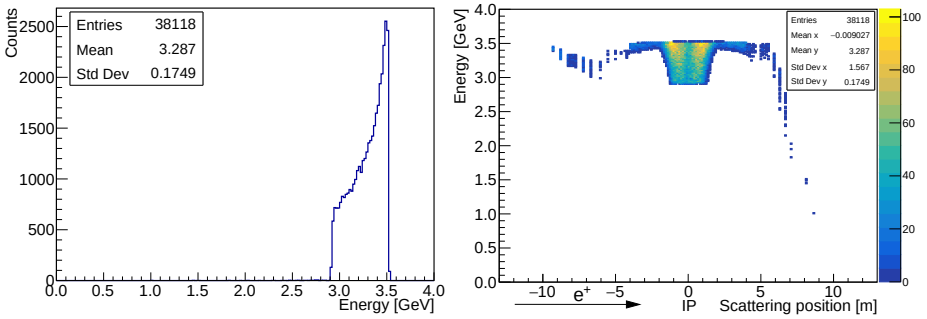

Figure 5: Simulated energy spectrum of Touschek positrons lost in the window on l.h.s and their relative rates (in arbitrary units) as function of energy and scattering position on r.h.s

3.1.2. Backgrounds measurement

Beam currents and vertical beam sizes were deliberately varied in dedicated experiments for the purpose of studying the Bremsstrahlung and Touschek background rates. For Bremsstrahlung, as shown in Figure 6, the LER beam current in LER was increased from 0 mA to 110 mA, in three steps. Clear corresponding changes in the monitors' signals: TIL(A) and TIL(C) could be observed.

The measured vacuum pressure was served to calibrate the simulated vacuum profile from [25] around the IP which was used to rescale the simulated results and compare with the experimental data. Simulated and measured signals data as a function of the product of beam current and vacuum pressure are shown

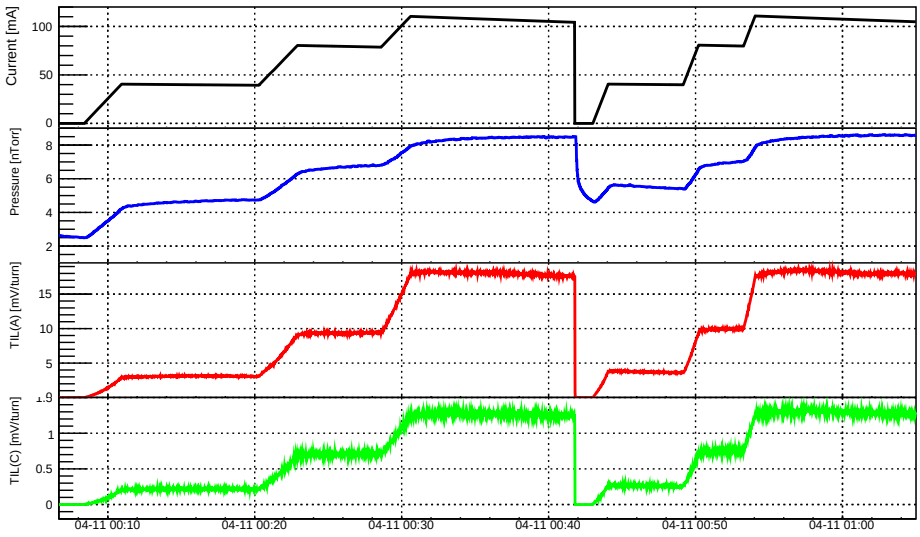

Figure 6: Example of background study in the LER: beam current was increased from 0 mA to 110 mA in three steps

in Figure 7. The simulation is about 11% higher than the measurements in the LER, which may be a measure of the reliability of the simulated vacuum pressure near the IP where it was shown to dominate the Bremsstrahlung rate.

According to the characteristics of Bremsstrahlung and Touschek processes, the background signals can be expressed as:

$$S_{bkgd} = S_{bg} * IP_eZ_e^2 + S_T * \frac{I^2}{\sigma_y} \tag{1}$$

Where S_{bkgd} is the measured signal, S_{bg} is a constant of proportionality of Bremsstrahlung sensitivity, S_T is the Touschek sensitivity, I is the beam current, P_e is the effective pressure and σ_y is the vertical beam size at the scattering position, which is proportional to the beam size measured by the X-ray monitor [26], $\sigma_y = \sqrt{\beta_y/\beta_{X-ray}}\sigma_{Xray}$. S_{bg} and S_T should be constant for the same lattice. For visualization purpose, it is more convenient to use Equation 2 and plot $\frac{S_{bkgd}}{IP_eZ_e^2}$ as function of $\frac{I}{P_e\sigma_yZ_e^2}$. With such a plot, the data should fall on a line with an offset indicating the Bremsstrahlung sensitivity S_{bg} and a slope

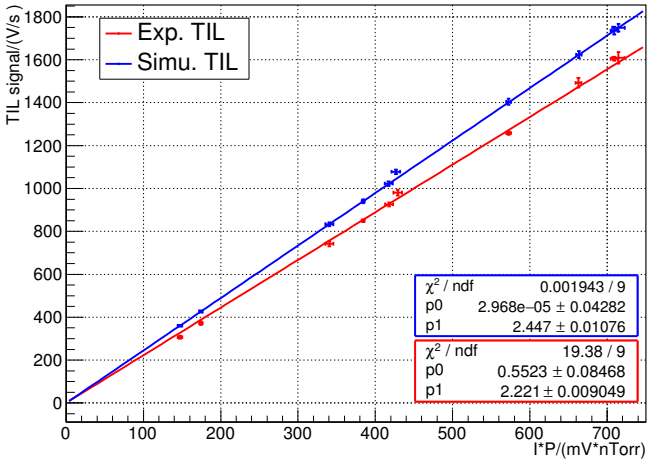

Figure 7: Comparison between simulated background signal and experimental data in the LER

equal to the Touschek sensitivity S_T.

$$\frac{S_{bkgd}}{IP_eZ_e^2} = S_{bg} + S_T * \frac{I}{P_e\sigma_y Z_e^2} \tag{2}$$

A "Touschek study" based on varying the vertical beam size was done at the end of the Phase-2 commissioning (with $\beta_x^* = 200$ mm and $\beta_y^* = 3$ mm in the LER) by changing the vertical emittance knob [27], which enable extracting the Touschek component present in our background, see Figure 8. The linearity of this distribution despite variations in current, pressure and horizontal beam size validates the hypothesis that the background signal mainly consists of Bremsstrahlung and Touschek processes. The offset of the fitted line contains the Bremsstrahlung contribution, and the slope indicates the change in the Touschek contribution as the beam size is varied. The moderate slope and relatively large offset indicates that the Bremsstrahlung process dominated in the background signals in our detectors in the LER during the Phase 2 commissioning.

From fitting the data, S_{bg} is about 24.45 and S_T is about 9.10. For the nominal beam conditions, with beam sizes of typically 50 μm measured by the X-Ray monitor [26], $S_{bkgd}/(IP_e)$ is about 28 $[mVnTorr^{-1}mA^{-1}]$, the contribu-

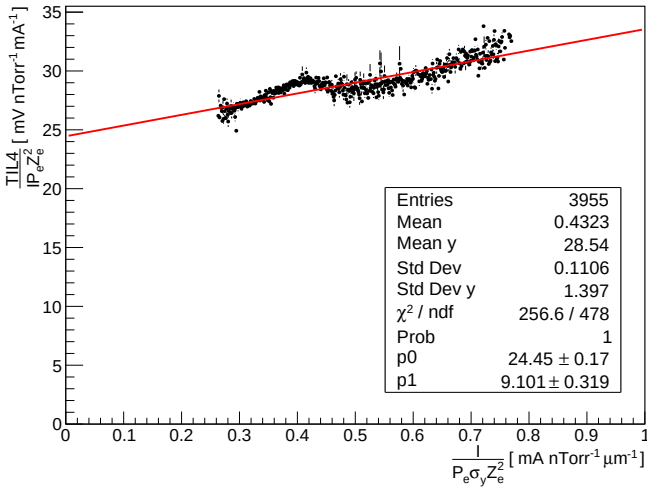

Figure 8: An example of fitting of Equation 2 on experimental data with different values of the vertical beam size in the LER. The offset of the fit line contains the Bremsstrahlung contribution, and the slope indicates change in the Touschek contribution as the beam size is varied.

tion from Bremsstrahlung is about 24.45 $[mVnTorr^{-1}mA^{-1}]$ and therefore that from the Touschek process should be close to 3.55 $[mVnTorr^{-1}mA^{-1}]$. That means the Bremsstrahlung and Touschek processes contribute about 87% and 13% of the background rate in our detectors, respectively. The corresponding fractions obtained with the simulation are 89% and 11%, which are in reasonable agreement with the measured values.

3.2. Luminosity signal simulation

The radiative Bhabha process at vanishing scattering angle

$$e^+ + e^- \rightarrow e^+ + e^- + \gamma \tag{3}$$

is used for the fast luminosity monitoring of the luminosity because of its large cross section. It was simulated with the GUINEA-PIG++ software [15] taking into account the parameters of both beams. Then scattered Bhabha positrons were tracked from the IP to the detector's position in the LER using the SAD software [16]. Figure 9 shows the energy spectrum of the Bhabha positrons at

the IP (green), lost on the beam pipe window (red), and the horizontal position as function of the positron energy at the position of the beam pipe window.

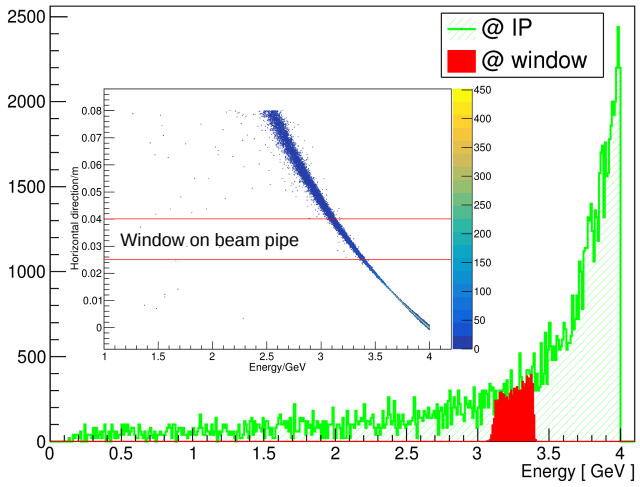

Figure 9: Energy spectrum of Bhabha positrons in LER produced at the IP (green) and lost on 45° beam pipe window (red). Distribution of horizontal position as function of the scattered positron energy at the position of beam pipe window (inserted plot)

A standalone GEANT4 model was set up to simulate the energy deposition in the diamond detectors, including the full dimension and detailed materials of the beam pipe, Tungsten radiator and the detectors, see Figure 10. The Bhabha scattered positrons lost on the beam pipe window were used as input.

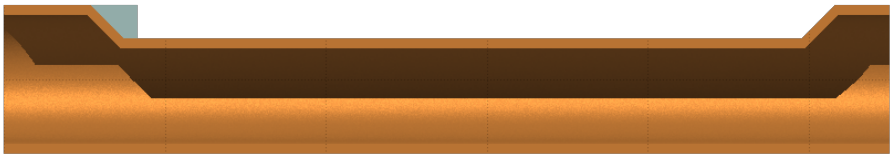

Figure 10: Sectional view of GEANT4 model of window shape beam pipe coupled with a Tungsten radiator of effective thickness 4*RL

Figure 11 shows the total deposited energy spectrum and the number of the secondary particles which deposit energy in the diamond detector located closest to the Tungsten radiator and beam pipe. The mean ionization energy is

around 13 eV to generate one electron-hole pair in diamond, and the broadband current amplifier used has a RMS noise level of 2.5 mV ($\sim 10^4$ electrons). After implementing a threshold of four times of the RMS noise, the overall detection efficiency is about 0.94%. This efficiency decreases by one order of magnitude for the detector located 10 cm away downstream.

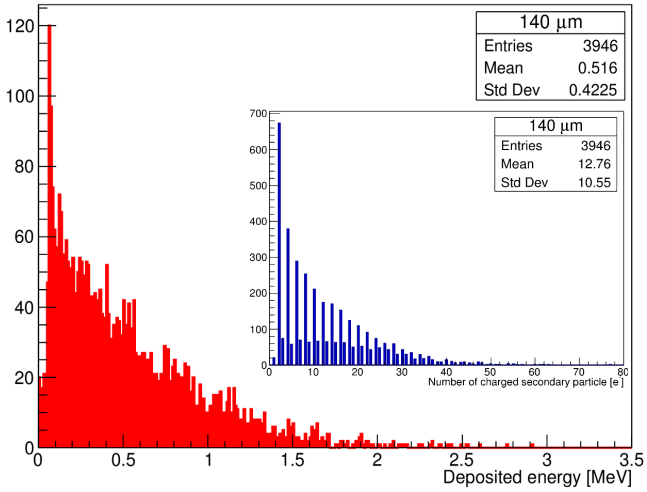

Figure 11: Energy deposited and number of charged secondary particles per Bhabha positron in diamond detector located closest to the Tungsten radiator and beam pipe

3.3. Luminosity measurements

Whenever beams were colliding during the Phase-2 commissioning, both train integrated luminosity signals (TIL) and bunch integrated luminosity signals (BIL) were provided.

3.3.1. Train integrated luminosity signals

Train integrated luminosity signals integrate the signal amplitude over all the bunches in 1 ms to meet the needs of the dithering feedback system. In the mean time, accumulation of this luminosity signal over 1 s was also processed to provide the relative luminosity information to the SuperKEKB control room, which is quite useful for collision tuning and related studies. As shown in Figure 12, in general, the luminosity signals (TIL in LER (A and C)) follow the

change of the product of beam currents in both rings. During the continuous injection period (17:00∼22:00), luminosity signal changes were larger than the beam current variations due to varying offsets between the two beams, caused for instance by vibrations of mechanical supports driven by the ground motion, especially in the vertical direction.

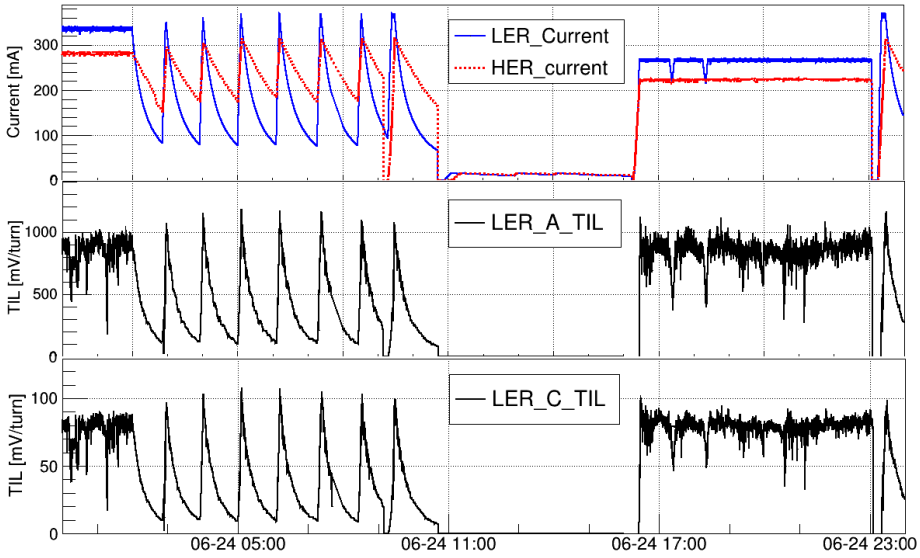

Figure 12: Example of the measured luminosity signals (LER) together with beam currents in both rings, sampled every 1 s over a day

The luminosity signals in the LER from channel A and C have the same trends, the only difference being their different distances to the Tungsten radiator. According to the GEANT4 simulation, the ratio of signals between the two channels is about 13.1. Figure 13 shows the relative luminosity signals from LER channel A and C plotted one against the other. An obvious linear relationship can be seen and the ratio between two channels is about 12.27, consistent with the simulation.

As a complementary device, the ZDLM, based on Scintillator and Cherenkov detectors, was also employed during the Phase-2 commissioning. Results from the two monitors (LumiBelle2 and ZDLM) were compared to check their performances. The result is shown in Figure 14 for the most sensitive diamond

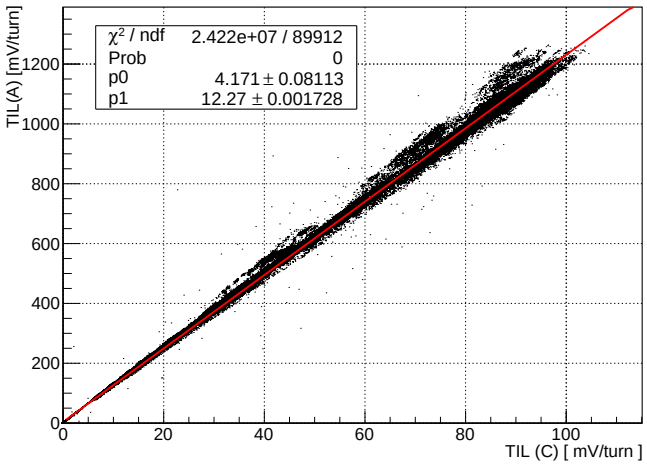

Figure 13: Luminosity signals from LER channel A against LER channel C

detector channel (Channel A). We notice that the relation between the two monitors is linear in the present luminosity range.

In addition to these two relative luminosity monitors, ECL, by measuring the coincidence rates in opposite sectors of the end-cap calorimeters of the Belle II detector for Bhabha events scattered with finite angles, provides an absolute value of the luminosity after proper calibration. To evaluate the performance of our relative luminosity monitors, the correlation between signals from the most sensitive channel in LER (LER A) and luminosity signals from ECL was checked, and the result is shown in Figure 15. As expected, our luminosity signals from Bhabha events at vanishing scattering angle are proportional to the absolute luminosity signals provided by ECL.

By checking the correlation of different channels of the monitors and with ZDLM and ECL, it's obvious that the monitors based on diamond detectors worked well and are consistent with other standalone luminosity monitors. This gives us confidence in using the 1 kHz luminosity signals as the input of the luminosity dithering orbit feedback system. Figure 16 shows the distribution of the luminosity signals from the most sensitive channel in LER (LER A) at 1 kHz, as well the raw data in the insert plot, the luminosity provided by ECL during that

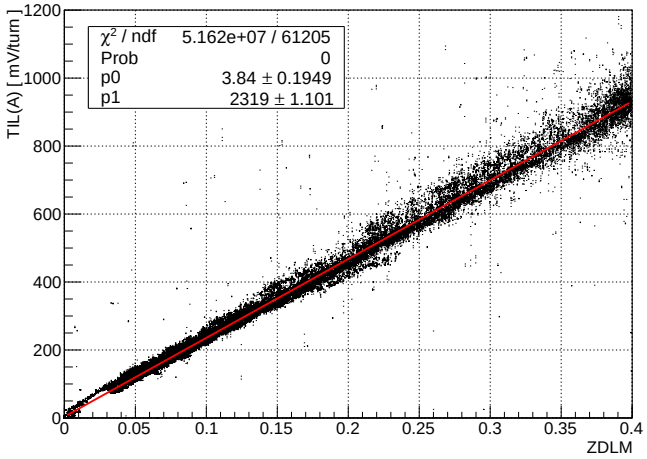

Figure 14: Luminosity signals from the most sensitive channel (LER A) against ZDLM in LER

period was about $(1.85\pm0.05)\times10^{33}\ cm^{-2}s^{-1}$. By studying the short term fluctuations in the 1 kHz TIL data for the most sensitive channel (LER A), during which period the luminosity was assuming to be close to stable, a conservative estimation of the relative precision of 2.3% can be obtained. This estimation is an upper bound, since possible genuine variations in luminosity during the short interval of time neglected. For the same luminosity, the predicted precision from our simulation based on Poisson statistics, was 2.0%. Possible explanations for the slightly different precisions obtained in the simulation and in data are, besides genuine luminosity fluctuation during the selected short period, differences in thresholds used for real and simulated data, imperfect peak detection, etc.

In addition, the relative precision of the 1 kHz luminosity signals with respect to the luminosity was also studied, as shown in Figure 17. It's clear that the relative precision improves with increasing luminosity. The proportionality of the relative precision to the inverse of the square root of luminosity supports our assumption of relative precision estimation based on Poisson statistics. It permits us to extrapolate the relative precision behavior to higher luminosities. For example, a relative precision of 1% can be expected for LER-A once the luminosity reaches $10^{34}\ cm^{-2}s^{-1}$ based on reasonable extrapolation.

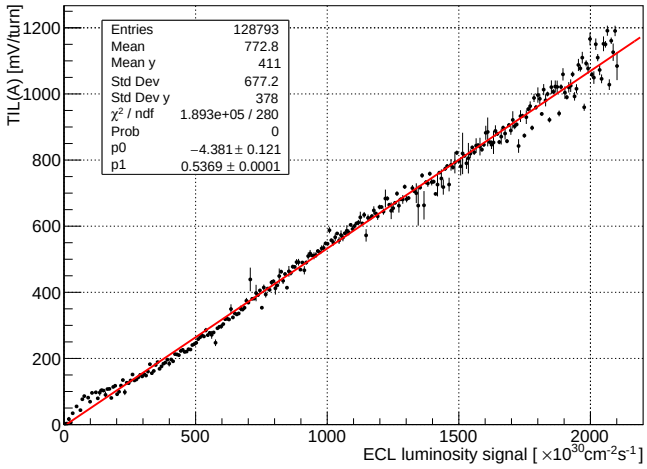

Figure 15: Luminosity signals from the most sensitive channel (LER A) against the absolute luminosity signals provided by ECL

3.3.2. Bunch integrated luminosity signals

With a large number of bunches populating the ring, up to 2500 bunches/turn in the nominal case, variations in the bunch transverse positions and sizes are in principle possible through a variety of effects, causing systematic reduction in luminosity for some of the bunches, and should be monitored, just like the bunch currents. After getting the BIL sums for 5120 buckets, and comparing with the fill pattern of the machine, a display of the integrated luminosities per bunch could be obtained, as shown in Figure 18. The beam conditions were those at the end of Phase-2 commissioning, when the instantaneous luminosity was about 1.6×10^{33} $cm^{-2}s^{-1}$, with 395 bunches circulating in each ring, separated by 24 ns. The observed spread in bunch integrated luminosity signals was about 9.3%, dominated by the measured spread of the products of bunch currents, which was found to be about 8.7% using the bunch-by-bunch current monitor [28]. In comparison, the relative precision in the corresponding 1 kHz TIL data was 2.5%, from which the average relative precision of BIL signals at 1 Hz could be estimated at the level of 1.6% (by a simple scaling in the assumption of uniform bunch current and alignment of the bunches along the trains in

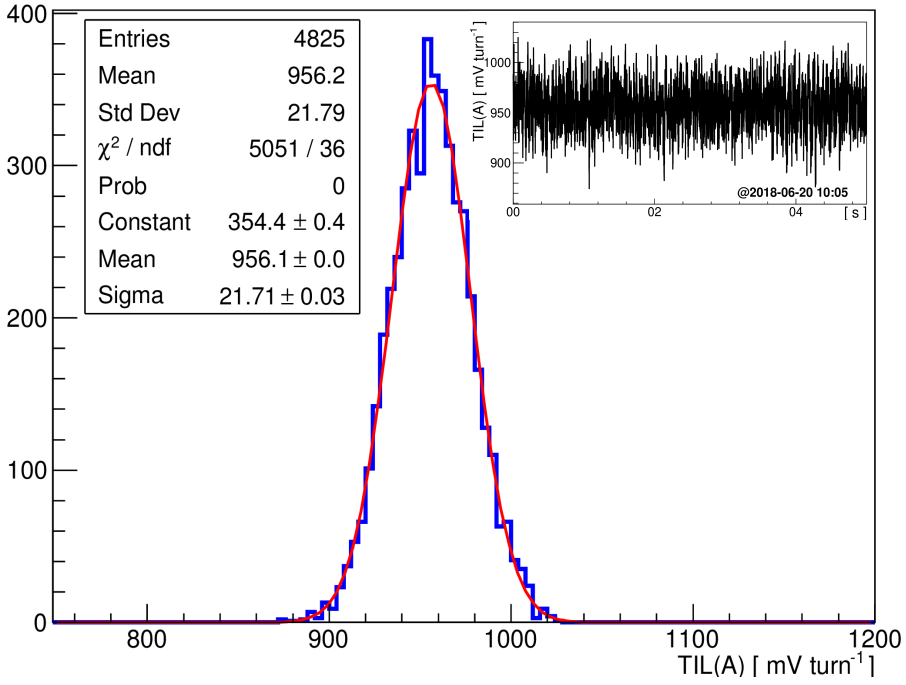

Figure 16: Distribution of luminosity signals at 1 kHz from the channel LER-A when luminosity is around $(1.85\pm0.05)\times10^{33}\ cm^{-2}s^{-1}$, raw data is shown in the insert plot

both rings).

4. Vertical beam size determination

By steering the electron beam while observing the signal changes of the luminosity monitor with extremely low beam current ($\sim$ 0.05 mA/bunch, for beam blow up effects induced by the beam-beam interaction to be negligible), both the optimum position in the vertical plane and the vertical beam size at the IP can be estimated. At the first beginning of collision tuning during Phase-2, such beam collision scans were used to put the beams into collision for the first time and to determine the optimum vertical position. Due to the large crossing angle of two beams, the projection of the bunch length in the horizontal plane should be considered as the effective horizontal beam size, which is much larger than the actual beam size, and out of the range of the local bumps at the IP

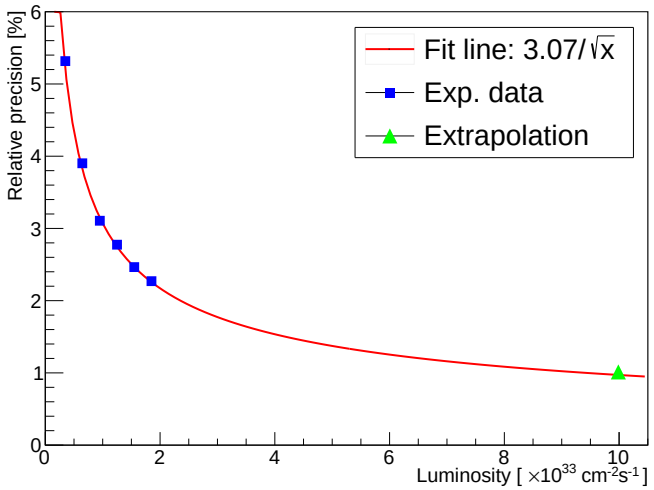

Figure 17: Relative precision of the 1 kHz luminosity signals from the most sensitive channel (LER-A) with respect to the luminosity

that steering magnets can produce. Therefore, the horizontal beam offset scan was not performed and unnecessary.

4.1. Averaged vertical beam size

Based on the changes in the train integrated luminosity signal, the averaged vertical beam size was estimated by vertical offset scanning. The data of Figure 19 is the relative train integrated luminosity signal as function of the vertical offset of the electron beam, taken at the end of Phase-2. Fitted by a Gaussian function, the standard deviation is Σ_y=0.51±0.01 μm, and fitted luminosity peak at 0.18 ± 0.01 μm.

With the assumption that the spatial distributions of the electron and positron beams are both Gaussian, the measured signal can be expressed as the convolution of the two beams:

$$L \sim Ae^{-(x-a)^2/2\sigma_{y,e^-}} \otimes Be^{-(x-b)^2/2\sigma_{y,e^+}} = Ce^{-(x-c)^2/2\Sigma_y^2} \qquad (4)$$

where L is the relative luminosity signals, $c = a+b$, $C = AB\sqrt{2\pi}\sigma_{y,e^-}\sigma_{y,e^+}/\sqrt{\sigma_{y,e^-}^2 + \sigma_{y,e^+}^2}$, and Σ_y^2 is the quadrature sum of the two vertical beam sizes at IP: Σ_y^2 =

$\sigma^2_{y,e^-} + \sigma^2_{y,e^+}$. Assuming that the vertical beam sizes of the two beams are equal, we have:

$$\sigma_y = \Sigma_y/\sqrt{2} = 0.36 \pm 0.01 \ \mu m \tag{5}$$

In addition, the electron vertical scan method can determine the optimum position where the luminosity is maximized in the vertical plane, corresponding to the peak position of Figure 19: $\bar{y} = 0.18 \pm 0.01 \ \mu m$. During SuperKEKB Phase-2 commissioning, this technique was used many times to search for collisions and to optimize the overlap of the two beams in the vertical plane. Other than the beam size determination and vertical offset optimization, the signal-to-noise ratio (SNR) could also be estimated, as the ratio of the luminosity signal at peak position and when the two beams were completely separated from each other. During this scan, the maximum luminosity provided by the ECL was $1.3\times\ 10^{32}\ cm^{-2}s^{-1}$ and the SNR from our monitor was about 65. Since in the future, luminosity improvement should mainly come from vertical β_y squeezing, SNR values larger than 100 can be expected when luminosity reaches 10^{34} $cm^{-2}s^{-1}$.

4.2. Bunch-by-bunch vertical beam size

Apart from the averaged vertical beam size based on train integrated luminosity signals, vertical beam sizes for individual bunches can also be estimated based on the bunch integrated luminosity signals during vertical scans. The same method as the averaged vertical beam size estimation is used. Figure 20 shows the results of the scanning for the four first bunches in the train, fitted by Gaussian functions. Similar to the averaged vertical beam size calculation described in 4.1, vertical beam sizes calculated for those four bunches are listed below:

$$\begin{aligned}
\sigma_{y1} &= \Sigma_{y1}/\sqrt{2} = 0.36 \pm 0.12 \ \mu m \\
\sigma_{y2} &= \Sigma_{y2}/\sqrt{2} = 0.36 \pm 0.12 \ \mu m \\
\sigma_{y3} &= \Sigma_{y3}/\sqrt{2} = 0.35 \pm 0.11 \ \mu m \\
\sigma_{y4} &= \Sigma_{y4}/\sqrt{2} = 0.36 \pm 0.09 \ \mu m
\end{aligned} \tag{6}$$

For the 754 colliding bunches during this vertical offset scan, the vertical beam sizes were calculated and the distribution is shown in Figure 21. As can be seen, it's distributed according to a Gaussian centered at 0.36 μm with a standard deviation of 0.01 μm. The averaged vertical beam size was 0.36 μm during this scan. The spread of the vertical beam sizes along the train is less than 2%.

Other than the vertical bunch beam size determination, the alignment of the bunches in the train is also an important quantity to evaluate the machine performance. As shown in Figure 22, the distribution of individual optimum positions for each bunch is also a Gaussian centered at 0.18 μm with standard deviation of 0.01 μm. The optimum position in the vertical plane fitted from the train integrated luminosity signals was 0.18 ± 0.01 μm, which is reasonably compatible with the optimum position of the individual bunches. In terms of the distribution of vertical optimum positions of the individual bunches, the alignment of the individual bunches have a relative precision of 4.43%, which combined with the machine parameters can allow studies of interactions between bunches, especially for high bunch currents and much smaller size beams, for example, for beams with parameters closer to the nominal ones expected during the upcoming Phase-3 commissioning period.

5. Conclusion and prospects

During Phase-2 commissioning of SuperKEKB, the luminosity monitor based on diamond detectors was installed and operated successfully. In the single beam commissioning, during which the monitor acted as a beam loss monitor, the background signals were measured and analysed, with results showing a good agreement with the detailed simulation. The Bremsstrahlung process dominated the background signal during Phase-2, with a fraction of 87%, while the Touschek process accounted for a fraction of about 13%. The good qualitative and quantitative agreement between the measurements and simulation enabled us to estimate the background level and SNR for the subsequent commission-

ing periods with colliding beams. After the first collisions were achieved, the diamond luminosity monitor played an important role in machine tuning during luminosity optimization. It provided several luminosity related observables: Relative train integrated luminosity signals at 1 Hz, giving direct feedback on the current luminosity to the SuperKEKB control system via EPICS for the machine tuning and study; Train integrated luminosity at 1 kHz, which was used as one of the inputs, along with the ZDLM signal, for the first tests of the dithering orbit feedback system to maintain an optimal horizontal offset between the two colliding beams; Bunch integrated luminosity signals at 1 Hz, which provide the relative luminosity information for each individual bunch. As a cross check, the luminosity signals from our monitor were compared with ZDLM and ECL. Good linearity between them prove that the luminosity monitor works well. Thanks to the 45° window and Tungsten radiator in the LER, the relative precision of the relative train-integrated-luminosity signal at 1 kHz is about 2.2% for a luminosity of $(1.85\pm0.05)\times10^{33}\ cm^{-2}s^{-1}$. 1% can be expected when luminosity reaches $10^{34}\ cm^{-2}s^{-1}$, which is precise enough as input to the dithering feedback system.

With the vertical offset scan technique, the beam size at the IP can be evaluated and the optimum position in the vertical plane can be found, which is very important during collision tuning at IP. In addition, the bunch integrated luminosity signals during the scans can also provide information on the vertical beam size and alignment for each individual bunch, which is quite useful for studying the potential variations along the bunch trains.

With the expected increases in luminosity and evolution of the machine in future years, some improvements and further studies are needed, in particular:

- Optimizing the combination and positions of detectors and amplifiers to ensure sufficient relative precision over the full range of expected luminosities from the lowest values during optical tuning to the nominal value, which corresponds to more than three orders of magnitude, while minimizing the radiation dose accumulating on the diamond detectors, to avoid

potential deterioration in their performance.

- Shielding to mitigate activation of the beam pipe and radiator on the LER side, which is expected to become relatively large at nominal luminosity.
- Equipping a new station for scattered Bhabha photon measurements on the HER side, where higher rates are predicted.
- Upgrading and maintaining the DAQ for long-term operation.

6. Acknowledgement

This work was supported in part by the China Scholarship Council (CSC), the H2020 European Commission RISE project E-JADE (contract No.645479) and the Toshiko Yuasa France Japan Particle laboratory (TYL-FJPPL), project A_RD_08. The authors would also like to express their warm thanks to K. Kanazawa, Y. Suetsugu, Y. Ohnishi and M. Tobiyama for their important support and advice all along the project, A. Fisher and U. Wienands for the useful comments and discussions on fast luminosity monitoring as input to dithering feedback system, BEAST group of the Belle II experiment for the useful comments, discussion and experience on background signal analysis, and the SuperKEKB commissioning group for their useful comments and discussion on the luminosity monitoring system.

7. References

[1] Y. Ohnishi, T. Abe, *et al.*, "Accelerator design at SuperKEKB," *Progress of Theoretical and Experimental Physics*, vol. 2013, no. 3, p. 03A011, 2013.

[2] K. Akai, K. Furukawa, and H. Koiso, "SuperKEKB Collider," *Nucl. Instrum. Meth.*, vol. A907, pp. 188–199, 2018.

[3] T. Abe *et al.*, "Belle II Technical Design Report," 2010.

[4] M. Masuzawa *et al.*, "Vibration issues for SuperKEKB," in *11th IWAA, DESY, September*, pp. 11–17, 2010.

[5] A. S. Fisher *et al.*, "Commissioning the Fast Luminosity Dither for PEP-II," *Conf. Proc.*, vol. C070625, p. 4165, 2007. [,4165(2007)].

[6] Y. Funakoshi *et al.*, "Interaction Point Orbit Feedback System at SuperKEKB," in *Proceedings, 6th International Particle Accelerator Conference (IPAC 2015): Richmond, Virginia, USA, May 3-8*, p. MOPHA054, 2015.

[7] C. Pang, P. Bambade, Y. Funakoshi, and S. Uehara, "Simulation study on luminosity feedback for horizontal beam stabilization at SuperKEKB," *Journal of Physics: Conference Series*, vol. 1067, no. 7, p. 072023, 2018.

[8] C. Pang, P. Bambade, *et al.*, "Preparation of CVD Diamond Detector for fast Luminosity Monitoring of SuperKEKB," in *8th International Particle Accelerator Conference*, (Copenhagen, Denmark), p. MOPAB027, May 2017.

[9] C. Pang, P. Bambade, *et al.*, "First Tests of SuperKEKB Fast Luminosity Monitors During 2018 Phase-2 Commissioning," in *9th International Particle Accelerator Conference*, (Vancouver, Canada), p. WEPAL038, Apr. 2018.

[10] F. Bachmair, "Diamond sensors for future high energy experiments," *Nucl. Instrum. Meth.*, vol. A831, pp. 370–377, 2015.

[11] CIVIDEC, *B1 sCVD diamond detector, C6 fast charge amplifier and C2 broadband current amplifier, https://cividec.at/.*

[12] R. Kleiss and H. Burkhardt, "BBBREM: Monte Carlo simulation of radiative Bhabha scattering in the very forward direction," *Comput. Phys. Commun.*, vol. 81, pp. 372–380, 1994.

[13] M. Masuzawa *et al.*, "Early Commissioning of the Luminosity Dither System for SuperKEKB)," in *Proceedings, 7th International Beam Instrument Conference (IBIC 2018): Shanghai, China, September*, p. TUPC13, 2018.

[14] V. E. Shebalin, "Electromagnetic Calorimeter of the Belle-II Detector," *Phys. Part. Nucl.*, vol. 49, no. 4, pp. 793–798, 2017.

[15] C. Rimbault, P. Bambade, O. Dadoun, G. Le Meur, F. Touze, M. C. del Alabau, and D. Schulte, "GUINEA PIG++ : An Upgraded Version of the Linear Collider Beam Beam Interaction Simulation Code GUINEA PIG," *Conf. Proc.*, vol. C070625, p. 2728, 2007. [,2728(2007)].

[16] "Strategic accelerator design." http://acc-physics.kek.jp/SAD/.

[17] S. Agostinelli *et al.*, "GEANT4: A Simulation toolkit," *Nucl. Instrum. Meth.*, vol. A506, pp. 250–303, 2003.

[18] C. Pang *et al.*, "Fast Luminosity Monitoring System at SuperKEKB," in *Proceedings, International workshop on the CEPC: Beijing, China, November 12-14*, 2018.

[19] D. El Khechen *et al.*, "First Tests of SuperKEKB Luminosity Monitors during 2016 Single Beam Commissioning," in *Proceedings, 7th International Particle Accelerator Conference (IPAC 2016): Busan, Korea, May 8-13*, p. MOPMB006, 2016.

[20] C. Pang *et al.*, "Fast Luminosity Monitoring for the SuperKEKB Collider (LumiBelle2 Project)," in *Proceedings, 7th International Beam Instrument Conference (IBIC 2018): Shanghai, China, September*, p. MOPA13, 2018.

[21] M. Iwasaki, Y. Ohnishi, S. Tanaka, T. Tsuboyama, K. Kanazawa, H. Nakayama, and H. Nakano, "Beam Background and MDI Design for SuperKEKB/Belle-II," *Conf. Proc.*, vol. C1205201, pp. 1825–1827, 2012.

[22] Y. Ohnishi, S. Tanaka, T. Tsuboyama, M. Iwasaki, K. Kanazawa, H. Nakayama, and H. Nakano, "Beam Background and MDI Design for SuperKEKB/Belle-II," *Conf. Proc.*, vol. C110904, pp. 3703–3705, 2011.

[23] Y. Ohnishi. Personal communication.

[24] P. Lewis, I. Jaegle, H. Nakayama, *et al.*, "First measurements of beam backgrounds at SuperKEKB," *Nuclear Instruments and Methods in Physics Research Section A: Accelerators, Spectrometers, Detectors and Associated Equipment*, 2018.

[25] M. Ady, R. Kersevan, and R. Leonid, *"Monte Carlo simulations of ultra high vacuum and synchrotron radiation for particle accelerators"*. PhD thesis, Ecole Polytechnique Frrale de Lausanne (EPFL), May 2016.

[26] E. Mulyani and J. Flanagan, "Calibration of X-ray Monitor during the Phase I of SuperKEKB commissioning," in *Proceedings, 5th International Beam Instrumentation Conference (IBIC 2016): Barcelona, Spain, September 11-15*, p. TUPG72, 2016.

[27] Y. Funakoshi, "Commissioning of SuperKEKB," in *Proceedings, 58th ICFA Advanced Beam Dynamics Workshop on High Luminosity Circular e^+e^- Colliders (eeFACT2016): Daresbury, United Kingdom, October 24-27*, p. MOOTH2, 2016.

[28] M. Tobiyama *et al.*, "Beam Commissioning of SuperKEKB Rings at Phase 1," in *Proceedings, 5th International Beam Instrumentation Conference (IBIC 2016): Barcelona, Spain, September 11-15*, p. MOAL03, 2016.

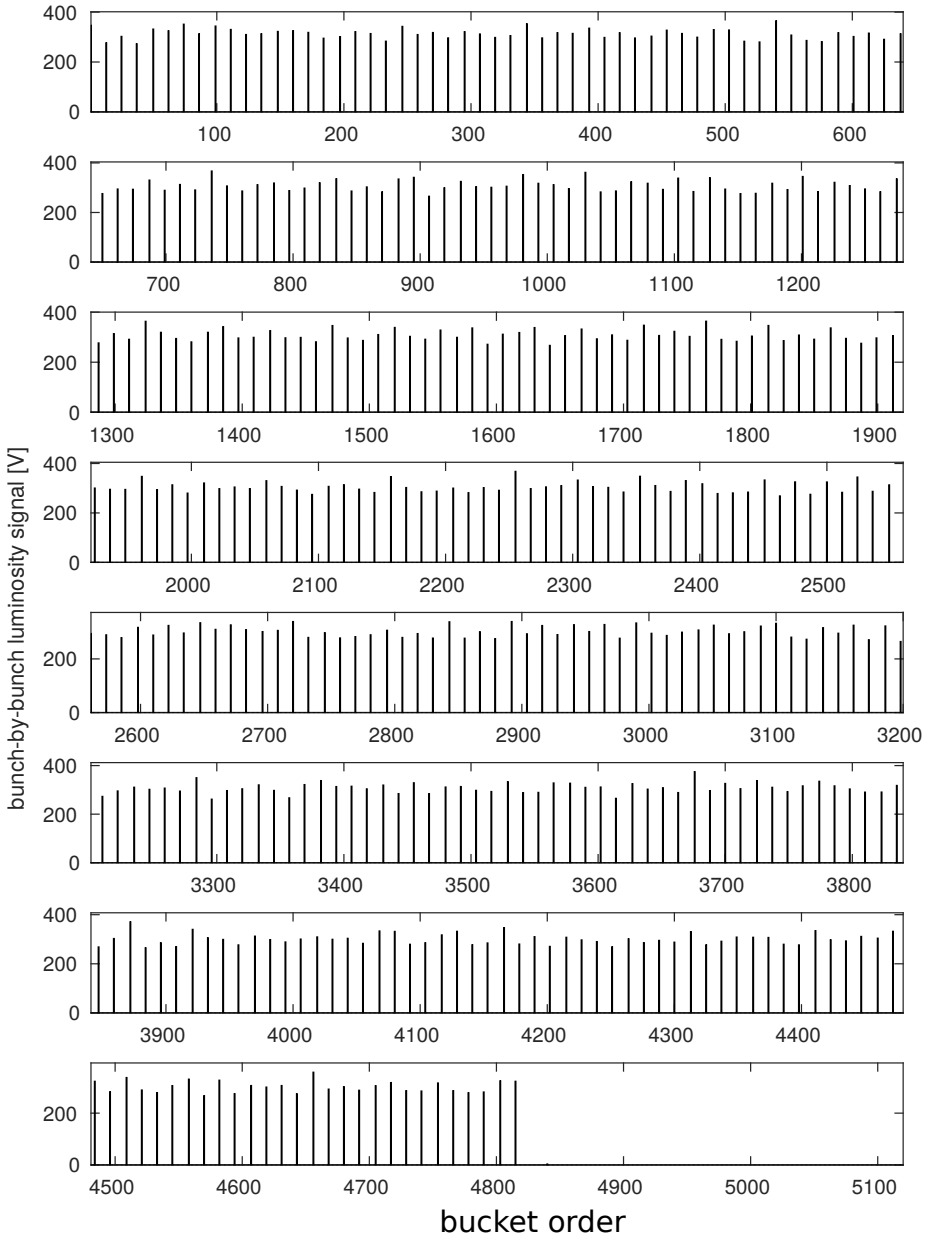

Figure 18: Bunch integrated luminosity signals, 395 bunches were stored in each of the SuperKEKB rings when this plot recorded

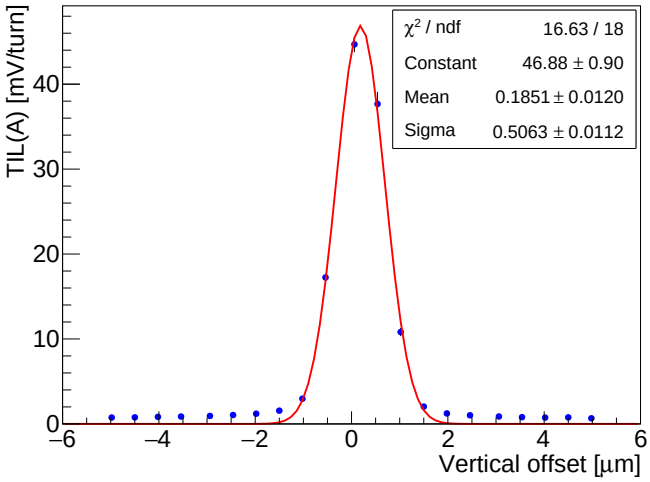

Figure 19: Relative train integrated luminosity signals with respect to the vertical offset of electron beam.

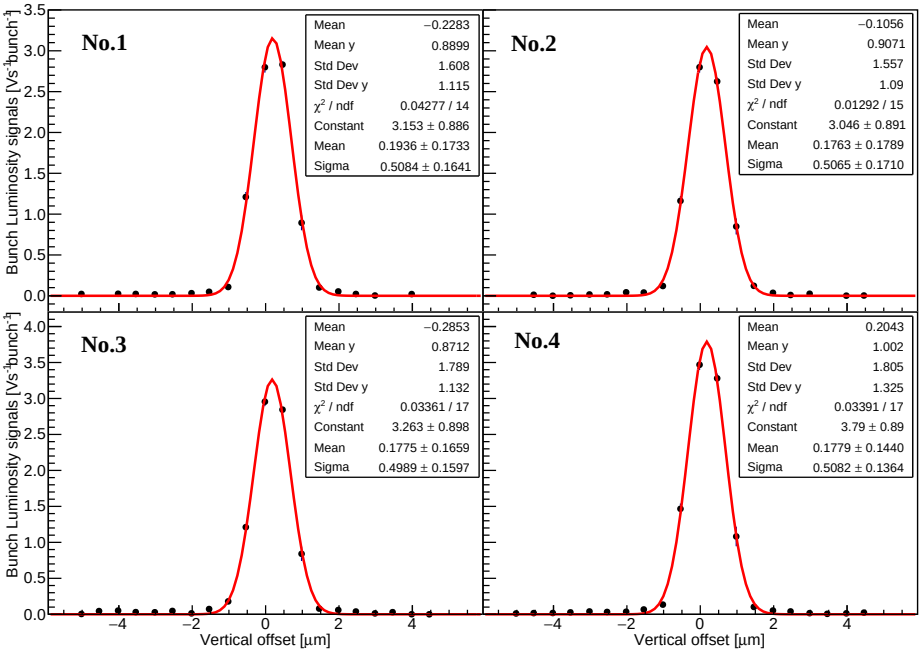

Figure 20: Example of relative bunch-integrated-luminosity signals as function of the vertical offset of electron beam: No.1-4 correspond to the four first bunches in the train.

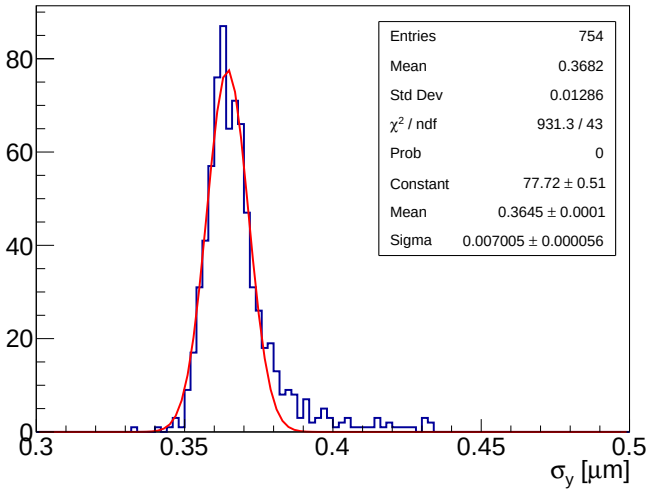

Figure 21: Distribution of vertical beam sizes for bunches along the trains.

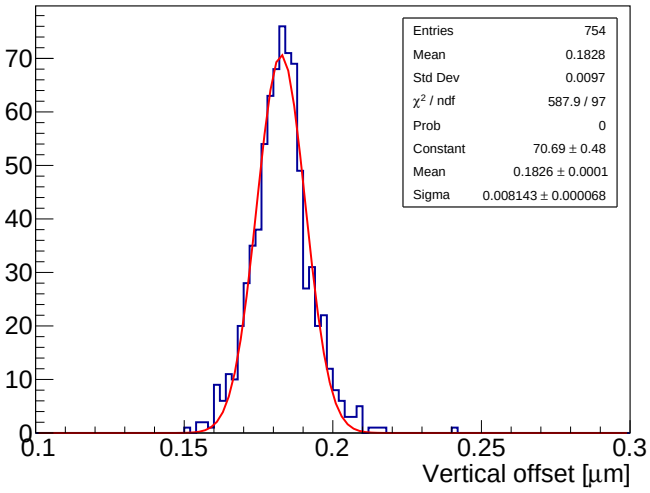

Figure 22: Distribution of optimum vertical position for the electron bunches corresponding to maximum bunch-integrated luminosities.